Chemosphere 252 (2020) 126523

Contents lists available at ScienceDirect

Chemosphere

journal homepage: www.elsevier.com/locate/chemosphere

Enhancing Chromium (VI) removal from synthetic and real tannery effluents by using diatomite-embedded nanopyroxene

Afif Hethnawi [a], Wisal Khderat [b], Kotaybah Hashlamoun [c], Amer Kanan [b], Nashaat N. Nassar [a, *]

[a] Department of Chemical and Petroleum Engineering, University of Calgary, Alberta, T2N 1N4, Canada
[b] Department of Earth and Environmental Science, Al-Quds University, P.O Box 20002, Jerusalem, Palestine
[c] Graduate Program in Biomedical Engineering, University of Calgary, Calgary, Alberta, T2N 1N4, Canada

HIGHLIGHTS

- Diatomite embedded nanopyroxene was effective in removing Cr(VI) from tannery effluent.
- Batch and column adsorption tests were conducted.
- Breakthrough curves were described by the dimensionless advection-dispersion transport model.

GRAPHICAL ABSTRACT

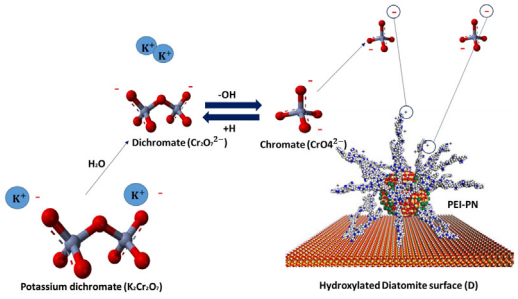

ARTICLE INFO

Article history:
Received 5 December 2019
Received in revised form
13 March 2020
Accepted 15 March 2020
Available online 18 March 2020

Handling Editor: Y Yeomin Yoon

Keywords:
Tannery wastewater
Chromium
Adsorption
Fixed-bed column
Dimensionless advection-axial dispersion model

ABSTRACT

A commercial filter aid material of Diatomite was modified via loading it with a low mass fraction of polyethylenimine-functionalized pyroxene nanoparticles (PEI-PNs) to enhance its adsorption activities. The modified Diatomite was then used for Cr(VI) removal from dichromate solution and from real tannery wastewater. For the synthetic wastewater, batch adsorption experiments were first performed at various pH and Cr(VI) initial concentrations. Then, the obtained kinetic parameters were used to investigate the continuous adsorption inside the fixed-bed column. The continuous removal of the Cr(VI) was performed inside a fixed-bed column under various influent flow rates, Cr(VI) initial concentrations, and bed-heights. In the column experiments, high adsorption of Cr(VI) was observed at low flow rates, high bed heights, and low influent initial concentrations. A dimensionless form of the advection-axial dispersion model, featuring Peclet number as a fitting parameter, was then used to study the break-through behavior under various dynamic parameters. Afterward, the modified Diatomite was used to remediate well characterized real tannery wastewater. For the treatment of the tannery wastewater, our modified filter aid, compared with the non-modified one, showed an outstanding performance and a higher removal efficiency.

1. Introduction

The leather tanning industry has a major relevance in the global economy, covering more than 50% of the leather demand (Benhadji

* Corresponding author.
E-mail address: nassar@ucalgary.ca (N.N. Nassar).

https://doi.org/10.1016/j.chemosphere.2020.126523
0045-6535/

et al., 2011; Elabbas et al., 2016; Fabbricino et al., 2013). It is recognized as a primary source of pollution, due to the large volumes of wastewater resulting from the use of various kinds of complex and hazardous raw materials involved in processing the final products (Wang et al., 2016; Nath et al., 2005). Thus, the effluent of leather tanning industry poses a serious environmental threat, especially when it contains high levels of salinity, organic load (chemical oxygen demand (COD) and biological oxygen demand (BOD)), inorganic matter, dissolved and suspended solids, ammonia, and some other pollutants (e.g., sulfide, chromium, chloride, sodium and other salt residues) (Wang et al., 2016; Nath et al., 2005; Lofrano et al., 2013; Saxena et al., 2016). Chrome tanning, as mostly adapted, is a process that performed for raw feedstocks materials like hides and animal skins to produce leather as a final product (Menderes, 2002; Chandrasekaran et al., 1999). Basically, chrome tanning is a transformation process of the perishable raw feedstock material into a durable one through chromium and other inorganic agents. During the tanning process, the function of chromium salt is to form, through complexation with the polypeptide collagen components of leather, a protective layer, which prevents water from penetrating the leather pores and, consequently, from putrefaction (Menderes, 2002; Chandrasekaran et al., 1999; Ball, 2007). Prior to the chromium tanning process, the leather takes up only 60–80% of applied chromium, and the rest is discharged into the sewage system, causing serious threats to the living organisms and to the environment in general (Wang et al., 2016; Nath et al., 2005; Menderes, 2002; Chandrasekaran et al., 1999; Ball, 2007). Excess chromium ions in the discharged liquid tanning wastewater are divided into two forms; trivalent Cr^{3+} and hexavalent Cr^{6+}. The hexavalent chromium form is 500 times more toxic than the trivalent form (Fabbricino et al., 2013). Although some investigators have successfully reduced the chromium contents of the wastewater effluent, by utilizing host treatment techniques, below the stipulated values, their techniques were costly ineffective and required using plenty of environmentally-harmful chemicals (Wang et al., 2016; Nath et al., 2005; Menderes, 2002; Chandrasekaran et al., 1999; Ball, 2007). Aber et al., for instance, suggested a treatment method by using electrocoagulation. Aber et al. achieved a high percentage of Cr (VI) removal from polluted solutions (Aber and Mirzajani, 2009). Nevertheless, electrocoagulation discharges huge amounts of sludge and byproducts. Moreover, it requires high operational and capital costs. In general, most of the reported techniques have some serious negative environmental impacts and some shortcomings and, therefore, extra attempts should be made into developing an effective, environmentally safe, low cost methods, for removing toxic pollutant from aquatic environments (Saxena et al., 2016). Adsorption, when combined with an appropriate wastewater treatment method, is considered an effective and versatile method for removing chromium ions (Li et al., 2016; Gheju et al., 2016; Shahrak et al., 2017). Many sorbents (e.g., wool (Yunden et al., 2019), olive cake (Calero, 2018) and charcoal (Agarwal and Gupta, 2015) showed a great performance for the removal of chrome. However, most of these sorbents, and even sorbents with larger surface areas (Stoquart et al., 2012; Mohan and Pittman, 2006), exhibited low adsorption capacity and slow process kinetic.

Recently, research has heavily involved the use of advanced nanoparticle technology in the area of water treatment. Nanotechnology holds the promise of creating new effective adsorbents, at the nanoscale, with high activity and large surface area per volume ratio (Shahrak et al., 2017). Nanoparticles have unique adsorption properties due to the presence of excellent distributions of active surface sites and surface multi-functionalities (Qu et al., 2013). Metal nano-oxides, unlike many adsorbents, have shown fast and superior adsorption removal capacity of various heavy metals from wastewater (Qu et al., 2013; Xu et al., 2012). However, applying such nanoparticles for water treatment can only be effective if they are stable under aqueous conditions (Qu et al., 2013; Xu et al., 2012). As a result, surface functionalization has been widely used to enhance nanoparticle stability, using various agents and polymers (Xin et al., 2012; Huang and Chen, 2009). Minimizing nanoparticle aggregation is achieved either by applying the chemical agents or polymers in-situ, where treatment is needed, or by loading a low mass fraction of nanoparticles into a support like clay, sand or Diatomite. In this study, polyethylenimine-functionalized nanopyroxene (PEI-PNs) were loaded into filter aid material of Diatomite, at low mass fraction, to provide a better dispersion of the nanoparticles, and to maintain a reasonable flux that would facilitate the regeneration of the spent materials after adsorption by backwashing (Hethnawi et al., 2017a, 2018). Loading a small mass fraction of nanomaterial into Diatomite converts it into a hybrid medium that is able to enhance the removal efficiency of the containment via adsorption. In the current study, we demonstrate the capability of the hydride filtration collector of Diatomite before and after loading with a small mass fraction of PEI-PNs in removing chromium ions from dichromate solution and real tanning wastewater, using both batch and fixed-bed treatment modes. In the batch adsorption study, we investigated the effects of pH and the initial concentration of chromium, to evaluate the equilibrium parameters. Afterward, for the fixed-bed column experiments, by involving the equilibrium parameters obtained from the batch experiments, we investigated the effects of dynamic parameters (e.g., flow rate, inlet concentration, and bed height). Finally, the obtained breakthrough profiles were described using a dimensionless convection-axial dispersion model.

2. Materials and methods

2.1. Diatomite loaded with nanoparticles

Diatomite (DICALITE 4500, Dicalite Minerals Corp., Burney, CA, USA) loaded with polyethyleneimine-functionalized pyroxene nanoparticles (PEI-PNs) at low mass percentage (<5 wt%) nanoparticles was synthesized following our previous work (Hethnawi et al., 2017b). In brief, the preparation of nanopyroxene was accomplished following the solution-gel method as reported in our previous studies (Hethnawi et al., 2017b; Hmoudah et al., 2016). Here the pyroxene nanoparticles were generated from a hydrothermally treated gel of iron silicate. The gel was prepared through mixed acid solution of iron and basic solution of silica. The acid solution was composed of 18.067 g of sulfuric acid (95–98%), 90 g of deionized, and anhydrous iron tri-chloride (97%wt). The silicate solution contained 21.42 g of sodium hydroxide (99.99%), 60 g of deionized water, and 30.70 g of sodium silicate ((10.6%) Na_2O, and (26.5%) SiO_2). After mixing, a hydrothermal crystallization for the resulting gel was performed at mild conditions inside a 300-mL reactor vessel for 72 h before washing the treated gel and recover the nanopyroxene. The recovered nanomaterials were directly added to 1.6 wt% of polyethyleneimine (PEI) for functionalization at room temperature without surface modifications. Then, 1 g of the functionalized nanoparticles were mixed with 19 g of Diatomite and 100 mL deionized water inside 200-mL glass bottle for 15 min. After that, the mixture was dried under vacuum, forming Diatomite embedded with PEI-PNs, noted as D-PEI-PNs at 5 wt%. Neat Diatomite was also used as adsorbent for comparison purposes. Table 1 lists a summary of obtained characterization results for PN, PEI-PN, Diatomite, and D-PEI-PN as reported from our previous study (Alnajjar et al., 2019). The charchterization results include the Brunauer–Emmett–Teller (BET) surface areas (m^2/g) and crystaline

Table 1
Summary of the obtained characterization results for PN, PEI-PN, Diatomite, and D-PEI-PN (Hethnawi et al., 2017b).

Material	BET surface area (m^2/g)	Crystaline size domain (nm)
PN	179	10.0 ± 2
PEI-PN	118	10.0 ± 2
Diatomiate (D)	0.31	25.5 ± 3
D-PEI-PN	12.04	45.5 ± 3

domain sizes (nm) of the previously mentioned materials. As shown, the surface area of PN was reduced via functionalizing the surface with PEI due to coating the nanoparticle surface with the polymer, while the crystaline domain sizes were unchanged with functionalization. Also, the surface area and crystaline domain size were enhanced for the Diatomite through loading the surface with 5 wt% of nanoparticles. Presence of PN on the Diatomite surface and the change in Diatomite structure through loading the nanoparticles were analyzed by field emission Quanta FEG 450 scanning electron microscopy) SEM) and high-resolution transmission electron microscope (HRTEM). Fig. 1 shows HRTEM images that were obtained for the Diatomite before (Fig. 1a) and after loading its surface with PEI-PN (Fig. 1b). As shown, HRTEM observation of Diatomite before the surface modifications exhibit smooth clean surface with seriate edge (Fig. 1a1 and 2). Also, certain Diatomite frustules display a high density of regularly ordered pores that are rigid in shape, and occasionally arranged in parallel sets with uniform pore spaces giving a honey-comb structure. Fig. 1b1 and 2 show clearly the structural changes in presence of low crystallinity nanoparticles. The micrographs of the same samples were also analyzed by SEM (Fig. 2). In the absence of nanoparticles, Diatomite with an amorphous silica structure is recognized (Fig. 2a). However, Diatomite frustules were partially modified with a good distribution of nanocrystals of PEI-PN (Fig. 2b). Pyroxene nanoparticles (PN) have negatively charged iron bonded to positively charged PEI (primary and secondary amine groups), resulting in a positively charged surface, indicating a strong capability of the functionalized nanoparticles to electrostatically adsorb negatively charged pollutants (e.g., dichromate). Accordingly, modifying the Diatomite surface with such functionalized nanoparticles can create a strong affinity towards removing the chromium ions from the dichromate and tannery wastewater solutions.

2.2. Adsorbate

Potassium dichromate ($K_2Cr_2O_7$, 99%) purchased from Sigma Aldrich, Ramallah, Palestine, and used as the source of chromium. Real tannery wastewater sample was obtained from the main drainpipe of a local tannery (AL-Fahis tannery, Hebron, Palestine) in July 2, 2018 in a pre-washed dried tightly capped glass container and kept stored in a dark incubator at 23 °C prior to analysis, which was performed immediately after stabilization. Then, the metal composition of the collected sample was measured by using the inductivity coupled plasma atomic emission spectroscopy (ICP-OES, Thermo Scientific ICAP series) analysis followed by Fourier transform infrared spectroscopy (FTIR) analysis. Calibration curves for Chromium, Lead, and Nickel detections by ICP were built using

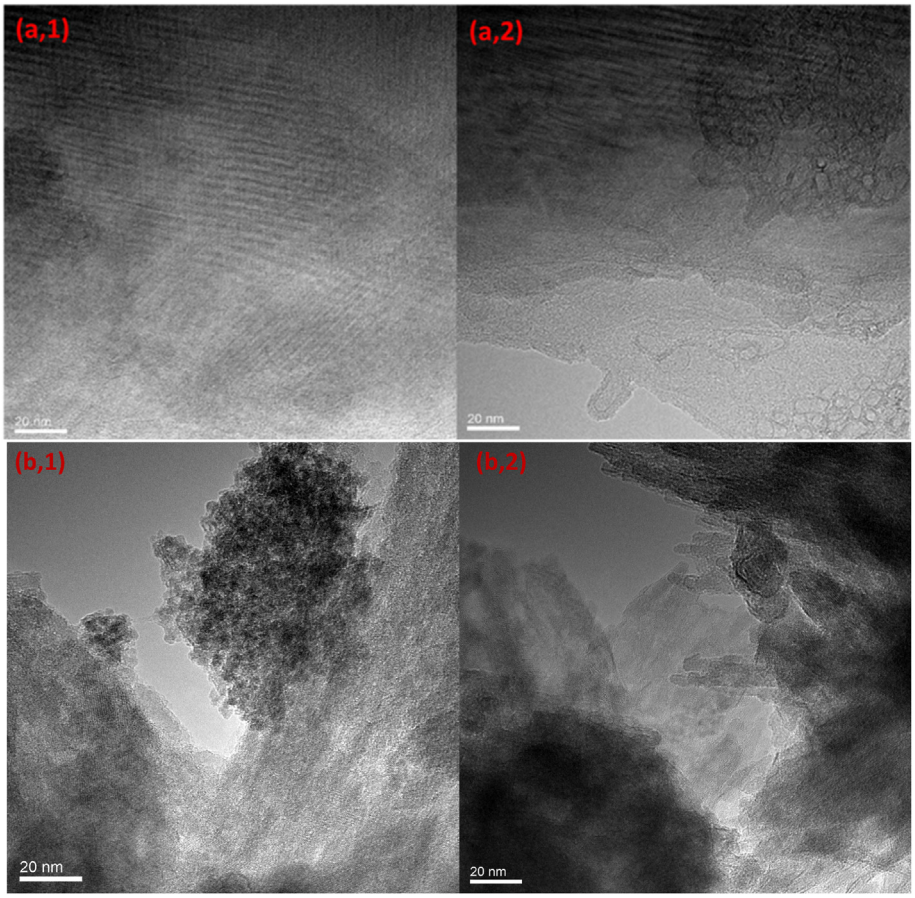

Fig. 1. HRTEM for the Diatomite before (a, 1and 2) and after anchoring PEI-PN (b, 1and 2). Line marks in the image corresponds to 20 nm.

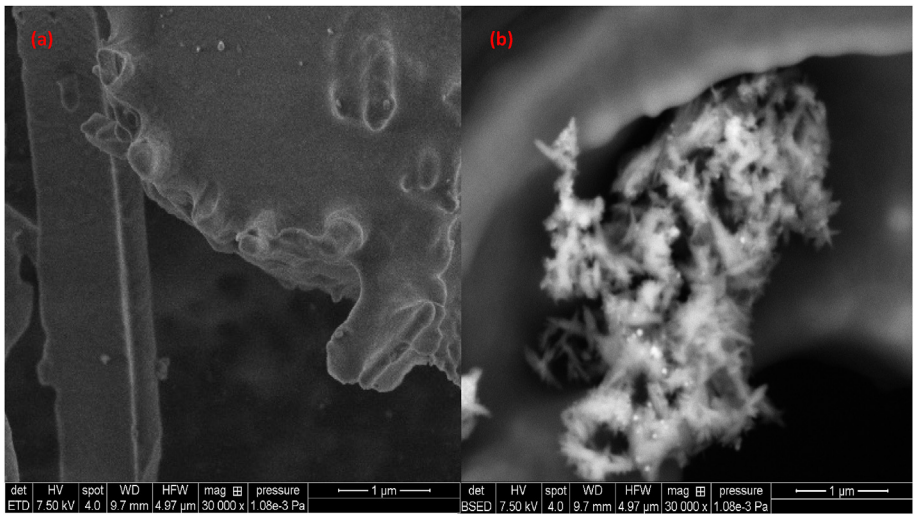

Fig. 2. SEM images for Diatomite before (a), and after anchoring PEI-PN (b). Line marks in the images corresponds to 1 μm.

Dashboard-iCAP with ASX560. For the calibration curves, standard solutions for the aforementioned metals were used, which were purchased from Sigma Aldrich at purities of 99.5, 98, and 99.5%, respectively. The FTIR analysis was conducted by an IRAffinity-1S instrument that was manufactured by Shimadzu Corporation. The analysis was operated in a diffuse reflectance mode in the range of 4000-400 cm^{-1} with a 4 cm^{-1} resolution and spectrum average scans of 50. Potassium bromide was used for dispersing the powder sample (2 mg per 200 mg, 1%wt/wt).

2.3. Batch adsorption experiments

To test the capability of Diatomite loaded with PEI-PNs (D-PEI-PNs) towards removing chromium ions from the dichromate solution, a series of batch adsorption experiments were conducted at 298 K. All the batch experiments were performed in 20 mL glass vials, such that 100 mg of D-PEI-PNs was added to each vial. For adsorption isotherm study, each vial was loaded with 10 mL of different initial concentration of chromium, ranged from 10 to 200 mg/L. The vials were tightly sealed and shacked on a platform shaker (New Brunswick Scientific, model: Innova 2300) at 200 rpm for 4 h, enough time to attain the equilibrium. After that, the samples were left on the bench over night to allow the adsorbent to settle. Then, the supernatant was decanted, and filtered through 0.45 μm syringe filter (Sterlitech, Kent, WA, USA). The residual chromium concentration in the supernatant was measured using UV–vis spectrophotometry (SL-218, UV–vis spectrophotometer, ELICO Ltd, Hyderabad, India) using a wavelength (λ_{max}) of 470 nm. A calibration curve of the UV–vis absorbance at 470 nm against the standard chromium concentrations was established, such that the absorbance of each standard solution was measured and correlated with its concentration in a linear relationship that represents concentration against absorbance. The calibration curve then was used to estimate the concentration of each sample before and after adsorption, allowing to calculate the percentage removal and adsorbed amount of chromium following equations (1) and (2), respectively. For the case of real wastewater sample, the supernatant was also analyzed for nickel (Ni) and lead (Pb) concentrations using an inductively coupled plasma-atomic emission spectroscopy (ICP-OES).

$$\%\ Removal\ of\ Cr = \frac{C_{initial} - C_{final}}{C_{initial}} X100\% \quad (1)$$

where $C_{initial}$ and C_{final} are the concentrations of chromium solutions before and after the batch adsorption experiments, respectively. The adsorbed amount of chromium ions (mg of chromium per g of adsorbent) was calculated as shown in Equation (2):

$$q = \frac{V}{m}(C_o - C) \quad (2)$$

where V, m, C_o and C are the volume of adsorbent (mL), mass of adsorbent (g), the initial concentration in solution (mg/L), and the final concentration (mg/L), respectively. For equilibrium data, C_e replaces C_o, and q_e replaces q in Equation (2). Langmuir-Freundlich combined model (Sips model) represented by Equation (3) (Hamdaoui and Naffrechoux, 2007; Foo and Hameed, 2010) was used to describe the adsorption isotherm.

$$q_e = \frac{k q_m C_e^n}{1 + k C_e^n} \quad (3)$$

where k, q_m, and n are Sips equilibrium constant $(L/mg)^n$, maximum adsorption capacity (mg/L), and heterogeneity coefficient (dimensionless) that express the sensitivity of the model towards Langmuir or Freundlich models. The model tends to be fully Langmuirian if the n value is equal 1.0. Having zero value of n suggests Freundlich isotherm model (Hethnawi et al., 2017a).

For the pH-dependent studies, chromium adsorption experiments were carried out at 298 K and 200 rpm for 24 h of mixing in a platform shaker. Aliquots of HNO_3 or NaOH were used to adjust the pH over the range 2–12. The mixture was shaken for specified time intervals and samples were selected at predetermined time intervals and analyzed for chromium concentration. All experiments were performed in triplicates to ensure the results are reliable, and the standard deviations were calculated and presented.

2.4. Column adsorption study

Fixed bed column experiments were carried out at certain operational parameters. Fig. 3 shows a schematic representation of the considered experimental setup. The setup composes of a

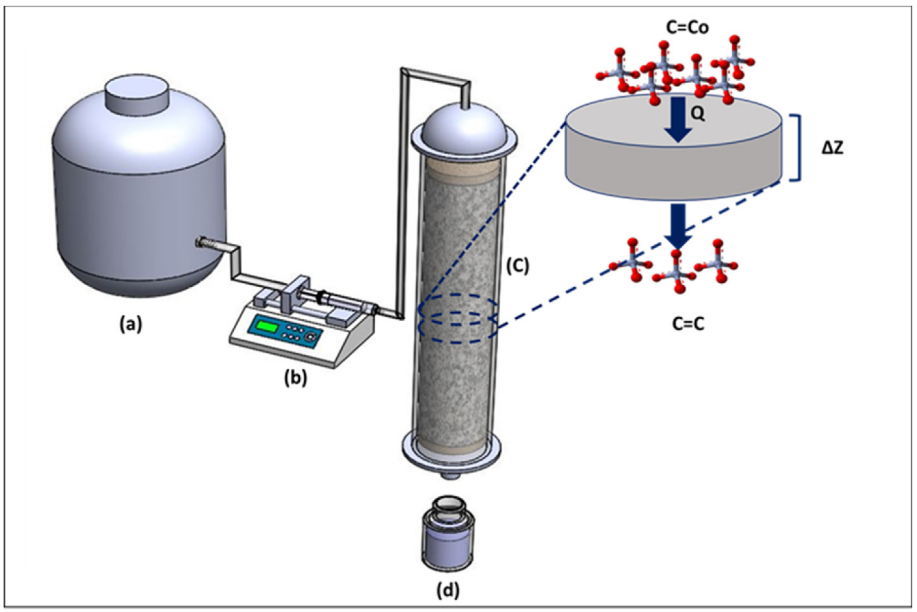

Fig. 3. Schematic representation of fixed-fixed bed column setup (not to scale) with the operating parameters of inlet chromium concentration (C_o), flow rate (Q) and bed height (Z): (a) chromium feed tank, (b) syringe pump, (c) fixed bed column, and (d) clean water sampling.

vertical glassy column with diameter and length of 0.9 and 15 cm, respectively. The setup also contains a storage tank connected to a syringe pump to feed the column with a controllable flow rates of wastewater solution. The adsorbent particles were packed in the column to the specified height. Two 1 cm cotton layers were placed at the bottom and top of the bed to improve flow distribution and to prevent escaping of adsorbent particles.

Each column experiment was performed by injecting the wastewater solution to the column in an upward mode, and the effluents were collected periodically from the bottom of the column. Then, the concentration was recorded at certain time intervals using UV–vis spectrophotometry. The flow was continuously provided till the breakpoint is reached, where the column is saturated and no significant difference between the inlet and outlet concentrations is noticed. Here, we carried out nine separate experiments to investigate the effects of four dynamic parameters, namely: type of adsorbent, inlet flow rate, inlet concentration, and bed height. Three different adsorbents (i.e., AC, Diatomite, and D-PEI-PNs) were tested under constant inlet flow (1 mL/min), initial concentration (200 mg/L), and bed height (7.5 cm) for comparison purposes. Then, the best adsorbent was selected and used to investigate the other operational parameters. Three runs were performed for each operating parameter, at three flow rates of (1, 1.5, and 2 mL/min), with chromium initial concentrations of (100, 150, 200 mg/L) and bed-heights (2.5, 3.5, and 7.5 cm). To validate the applicability of the D-PEI-PNs in removing chromium from real tannery effluent, two fixed bed experiments were carried out on real tannery effluent sample at initial chromium concentration of 200 mg/L, flow rate = 1 mL/min, and bed height = 7.5 cm for neat Diatomite and Diatomite loaded with PEI-NPs.

2.5. Column desorption experiments

To test the recyclability of D-PEI-PN, the spent material inside one saturated column was backwashed with an aqueous solution of HNO_3 (pH = 5) at a flow rate of 1 mL/min in downflow mode. For every cycle, the regeneration efficiency (ER%) is estimated by the following equation:

$$ER\% = \frac{q_{Tc}}{q_o} \times 100\% \quad (4)$$

where q_{Tc} and q_o are the total capacity for every cycle and the original capacity of the column, respectively.

2.6. Breakthrough analysis and modeling

In fixed bed adsorption, the concentrations in the fluid phase and the solid phase change with time. At first, most of the mass transfer takes place near the inlet of the bed, where the fluid contacts the adsorbent and the chromium ions get adsorbed forming a mass transfer zone at the entrance (Hethnawi et al., 2017a, 2018; Ghorai and Pant, 2005). This zone progressively moves downward with time to prevent attaining the equilibrium inside the column. When the mass transfer zone reaches to the bottom of the column, the breakpoint is obtained at which the inlet concentration over the outlet (C_t/C_o) is at around 0.05; where the time is identified as breakthrough time (t_b) (Hethnawi et al., 2017a, 2018; Ghorai and Pant, 2005). After t_b, the outlet concentration is gradually changed till the column gets nearly saturated at C_t/C_o of 0.95, where the saturation time (t_s) is obtained (Hethnawi et al., 2017a, 2018; Ghorai and Pant, 2005). Thus, plotting C_t/C_o against time forms breakthrough curve (BTC) that has a typical S-shape and the performance towards removing the chromium ions can be estimated by determination of designed parameters of the experimental breakthrough curves that are listed in Table 2. These parameters describe the performance of the adsorption bed through the obtained breakthrough curve data and are of importance for determining the dynamic behavior of the bed. The designed parameters shown in the table are the total time (t_t), useable time (t_u), length of unused bed (H_{UNU}), adsorbed quantity inside the column (q_T), amount chromium ions sent to the column (m_{total}), and percentage removal of chromium (%Removal) can describe the performance of the fixed-bed column toward removal of chromium. From the table also, H_T, C_o, C_t, Q, and t are the total bed height (cm), the inlet concentration in mg/L, the outlet concentrations in mg/L,

Table 2
Designed parameters of the experimental breakthrough curves.

Parameters	Equation	Reference
Total time (t_t)	$t_t = \int_0^{t_s}\left(1-\frac{C_t}{C_o}\right)dt$	(Hethnawi et al., 2017a, 2018; Ghorai and Pant, 2005)
The useable time (t_u)	$t_u = \int_0^{t_b}\left(1-\frac{C_t}{C_o}\right)dt$	(Hethnawi et al., 2017a, 2018; Ghorai and Pant, 2005)
The length of unused bed (H_{UNU})	$H_{UNU} = \left(1-\frac{t_u}{t_t}\right)H_T$	(Hethnawi et al., 2017a, 2018; Ghorai and Pant, 2005)
The adsorbed quantity inside the column (q_T)	$q_T = \frac{QC_o}{1000}\int_{t=o}^{t=t_{total}}\left(1-\frac{C_t}{C_o}\right)dt$	(Hethnawi et al., 2017a, 2018; Ghorai and Pant, 2005)
The amount chromium ions sent to the column (m_{total})	$m_{total} = \frac{C_o Q t_{total}}{1000}$	(Hethnawi et al., 2017a, 2018; Ghorai and Pant, 2005)
The percentage removal of chromium (*%Removal*)	$\%\ Removal = \frac{q_T}{m_{total}}\times 100$	(Hethnawi et al., 2017a, 2018; Ghorai and Pant, 2005)

the flowrate in mL/min and the time (min), respectively.

Furthermore, these parameters are helpful in finding the performance of certain adsorbents towards the removal of chromium ions, and their values are strongly influenced by manipulating some operational parameters like the inlet flow rate, influent initial concentration, and bed-height. In the pilot scale, the kinetic behavior of a fixed-bed column can be explained and the characteristic BTC of the adsorption phenomena can be obtained through mathematical models (Hethnawi et al., 2017a, 2018; Ghorai and Pant, 2005). In the earlier studies, the kinetics is described using a mathematical model that takes into account the external and internal mass-transfer resistances with a non-ideal plug flow behavior, without accounting for the axial dispersion along the column (Call et al., 2017; Malkoc and Nuhoglu, 2006; Aksu and Gönen, 2004; Han et al., 2007). However, presence of axial dispersion along the column is an important aspect, which has not been accounted for so far. In our previous studies, we developed an advection-axial dispersion model for explaining the kinetic behavior of adsorption phenomena incorporating the advection, axial dispersion, and the rate of adsorption along the column length as given by the following mass balance equation (Hethnawi et al., 2017a, 2018):

$$-D_L\frac{\partial^2 C}{\partial z^2}+u\frac{\partial C}{\partial z}+\frac{\partial C}{\partial t}+\rho_b\left(\frac{1-\varepsilon}{\varepsilon}\right)\frac{\partial q}{\partial t}=0, \quad (0<z<L,\quad 0<t<\infty) \tag{5}$$

where C is the concentration of the bulk adsorbate (mg/L), D_L is the axial dispersion coefficient (m/s^2), u is the interstitial velocity (m/s), q is the mass ratio of the adsorbed amount of adsorbate to the solid, z is the distance along the longitudinal axis of the bed (m), t is the time, ε is the bed porosity, and ρ_b is the bulk density (kg/ m^3). The contribution of each term, from left to right, is described as follows: axial dispersion, convection, transient term, and adsorption. In the adsorption term, assuming the obtained data are represented by the Langmuir model, (i.e., $n = 1$) in equation (3), then Equation (5) takes the final form

$$-D_L\frac{\partial^2 C}{\partial z^2}+u\frac{\partial C}{\partial z}+\frac{\partial C}{\partial t}+\rho_b\left(\frac{1-\varepsilon}{\varepsilon}\right)\frac{K\,q_m}{(1+K\,C)^2}\frac{\partial C}{\partial t}=0, \quad (0<z<L,\quad 0<t<\infty) \tag{6}$$

Due to the nonlinearity of the adsorption term, an analytical solution to this equation is difficult to find, if not impossible. Therefore, numerical methods are used. The only unknown parameter in Equation (6) is the dispersion coefficient, D_L, which can be found by fitting the experimental BTCs data with the numerical solution of Equation (6). The value of D_L could determine the dominating mass-transfer resistance (film or pore diffusion resistance) (Hethnawi et al., 2017a, 2018). However, D_L depends also on many geometrical parameters (e.g., the porosity and adsorbent particle size) and its order of magnitude is highly sensitive to the rate of adsorption as well as the variation of flow conditions, especially if scaling up is needed to an industrial field. Thus, combination of the phenomenological and geometrical parameters in dimensionless terms is more convenient to work with. Therefore, dimensionless analysis could be applied by one of two approaches: 1) we can solve the PDE, find the dispersion coefficient, and then calculate the dimensionless parameters; 2) alternatively, we can convert the PDE into a dimensionless form, solve it, and use the dimensionless parameter of interest as the fitting parameter. The second approach is more convenient and would result in less number of variables, in addition to the ability to scale up. For simplicity, we divide the analysis of the PDE into three steps: 1) Introducing the dimensionless parameters as required; 2) Rewriting the PDE in dimensionless form; and 3) Rewriting the initial and boundary conditions in terms of the dimensionless parameters, and then solving for the PDE. Table 3 lists the dimensionless parameters required for the PDE.

The differential terms $\partial C/\partial t$, $\partial C/\partial z$, and $\partial^2 C/\partial z^2$ have been replaced with their dimensionless counterparts as follows:

$$\frac{\partial C}{\partial t}=\frac{C_{in}\,D_L}{d_p^2}\frac{\partial \overline{C}}{\partial \overline{t}} \quad . \tag{7}$$

$$\frac{\partial C}{\partial z}=\frac{C_{in}}{L'}\frac{\partial \overline{C}}{\partial \eta} \quad . \tag{8}$$

$$\frac{\partial^2 C}{\partial z^2}=\frac{C_{in}}{(L')^2}\frac{\partial^2 \overline{C}}{\partial \eta^2} \tag{9}$$

By introducing these terms into Equation (6), and after rearrangement, one can obtain the following dimensionless equation:

$$-\frac{\partial^2 \overline{C}}{\partial \eta^2}+Pe_m\frac{\partial \overline{C}}{\partial \eta}+\frac{1}{r^2}\frac{\partial \overline{C}}{\partial \overline{t}}+\rho_b\frac{K\,q_m}{r\,(1+K\,C_{in}\,\overline{C})^2}\frac{\partial \overline{C}}{\partial \overline{t}}=0 \quad (0<\eta<1,\quad 0<\overline{t}<\infty) \tag{10}$$

Peclet number (Pe), which is a direct indicator of the rate limiting mass transfer phenomena (convection or dispersion), was used as the fitting parameter. The initial and boundary conditions that describe the process in Equation (5) are given by

$$C=0 \qquad (0<z<L,\quad t=0) \tag{11}$$

Table 3
Dimensionless parameters for the PDE in Equation (6).

Dimensionless Number	Description
$r = \left(\frac{1-\varepsilon}{\varepsilon}\right)$	Void ratio
$\mathrm{Sc} = \frac{\upsilon}{D_L}$	Schmidt number υ: kinematic viscosity
$L^{'} = \frac{d_p\,\varepsilon}{(1-\varepsilon)} = \frac{d_p}{r}$	Characteristic length of bed d_p: adsorbent diameter
$\overline{C} = \frac{C}{C_{in}}$	Normalized concentration
$\eta = \frac{z}{L^{'}}$	Dimensionless axial distance
$\overline{t} = \frac{D_L\,t}{{d_p}^2}$	Dimensionless time
$\mathrm{Re} = \frac{u\,d_p}{r\,\upsilon} = \frac{u\,L^{'}}{\upsilon}$	Reynolds number (Re)
$\mathrm{Pe}_m = \mathrm{Re} \times \mathrm{Sc} = \frac{u\,L^{'}}{D_L}$	Peclet number over the characteristic length (Pe_m)
$\mathrm{Pe}_L = \mathrm{Pe}_m\left(\frac{L}{L^{'}}\right)$	Peclet number over the real length of the column (Pe_L)

$$u(C_{in} - C) + D_L\frac{\partial C}{\partial z} = 0 \qquad (z = 0, \quad 0 < t < \infty) \tag{12}$$

$$\frac{\partial C}{\partial z} = 0 \qquad (z = L, \quad 0 < t < \infty) \tag{13}$$

The dimensionless forms for these conditions are

$$\overline{C} = 0 \qquad \left(0 < \eta < \frac{L}{L^{'}}, \quad \overline{t} = 0\right) \tag{14}$$

$$(1 - \overline{C}) + \frac{1}{Pe_m}\frac{\partial \overline{C}}{\partial \eta} = 0 \qquad (\eta = 0, \quad 0 < \overline{t} < \infty) \tag{15}$$

$$\frac{\partial \overline{C}}{\partial \eta} = 0 \qquad \left(\eta = \frac{L}{L^{'}}, \quad 0 < \overline{t} < \infty\right) \tag{16}$$

Hence, Equation (10) is numerically simulated in Mathematica software (v.10.2) and solved using Wolfram Mathematica package, with NDSolve command, using the Method of Lines by fitting the equation to the experimentally obtained breakthrough data. For each set of data, the proper value of Peclet number was found by minimizing the nonlinear error parameter χ^2. The error parameter, χ^2, is obtained by minimizing the sum squares of the difference between the experimental data and the numerical solutions (Coleman et al., 1991).

3. Results and discussion

3.1. Batch adsorption study

3.1.1. Initial pH effect

Initial pH effect is an important parameter that affects the adsorption of metal ions and controls the adsorption process. Many previous studies have reported pH variation effect on chromium uptake, and most of the studies have shown a remarkable decrease in the removal efficiency as pH increases. This adsorption behavior refers to the change of the surface charge and the degree of the adsorbent ionization after changing the medium pH (Hossein et al., 2019). However, The PEI-PN, as an active binding site within the Diatomite structure, tends to have a constant effect at various medium pH. In details, PEI-PN is composed of the PEI-functionalized nanoparticles as active binding sites. PEI on the nanoparticle surface has a wide range of buffering capacity (pH pKa) due to the presence of amino groups at every chain within the branched PEI, exhibiting positively charged surface at various pH (Hethnawi et al., 2017b). Thus, it is expected to have constant chromium uptake at various medium pH, which does not agree with the results obtained from the pH study (Fig. 4). Fig. 4 shows that increasing the pH value of the solution provided higher removal of chromium ions. In fact, varying the pH value not only influences the adsorbent surface, but also contributes to the ionization of the adsorptive molecules. As reported, the main ionic species in the solution at pH < 3 is by far Cr^{+3}, while for high pH, the chromate or dichromate anions are more prevalent. Thus, the pH was initially pre-adjusted at pH > 3 (Natale et al., 2015). Dissolving the $K_2Cr_2O_{7(s)}$ in an aqueous solution produces an anionic dichromate ($Cr_2O_7^{2-}$) and a cationic potassium ion (K^+), as the following chemical equation shows:

$$K_2Cr_2O_{7(s)} \rightarrow 2\ K^+_{(aq)} + Cr_2O_7^{2-}{}_{(aq)} \tag{17}$$

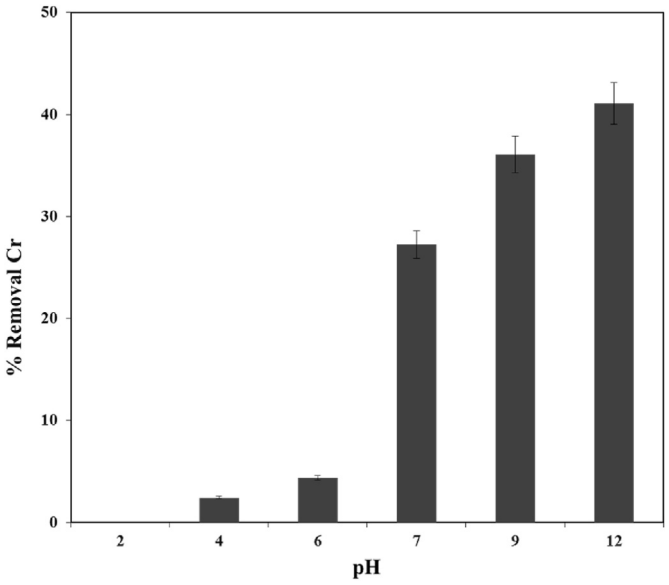

Fig. 4. Initial pH effect on chromium uptake at initial concentration of 200 mg/L and temperature of 20 °C.

Dichromate ion, $Cr_2O_7^{2-}{}_{(aq)}$, can be converted into a chromate ion, $CrO_4^{2-}{}_{(aq)}$ and conversely, according to the following equilibrium chemical equation:

$$Cr_2O_7^{2-}{}_{(aq)} + H_2O_{(aq)} \rightleftharpoons 2\ CrO_4^{2-}{}_{(aq)} + 2H^+{}_{(aq)} \quad (18)$$

The extent to which these reactions occur is dependent upon the concentration of the hydrogen ion, H^+ in the solution, which can be impacted by the addition HNO_3 and NaOH, causing a shift in the equilibrium according to Le Chatelier's principle (Cheung, 2007). As a result, increasing the pH will increase the concentration of CrO_4^{2-} in the aqueous solution, leading to more electrostatic interactions with the positively charged PEI-PN surface. Accordingly, a high pH medium is more favored for adsorption of chromate in the wastewater solution, and pH = 9 was chosen as the best operating pH for the adsorption process. Thus, the initial pH = 9 was the appropriate equilibrium and was used in all kinetic studies. Fig. 5 shows a schematic representation of the chemical structure of the repeated unites of the D-PEI-PN and their interaction mechanism with chromate groups at pH = 9.

3.1.2. Adsorption isotherm

By varying the initial concentration of chromium (VI) from 10 to 200 mg/L, the chromium removal by the adsorbent particles was studied in a batch process under pH of 9 and temperature of 298 K. The amount of chromium (VI) adsorbed in mg/g (chromium uptake) and the extent of removal for the adsorbents at equilibrium are shown in Fig. 6, which also includes the fitting of the equilibrium data (discrete points) with Sips model (continuous line). The corresponding fitting parameters of *K*, Q_m, and *n* were estimated to be 0.0001 $(L/mg)^n$, 14.2 mg/g, and 1.0, respectively. These fitting parameters were determined by applying a non-linear regression for the equilibrium data using OriginPro 8 SR4 software Version 8.095. The non-linear regression was achieved by minimizing the sum squares of the difference between the experimental data and those obtained from Sips model through manipulating the value of Chi-square (χ^2). The obtained value of χ^2 was around 0.012,

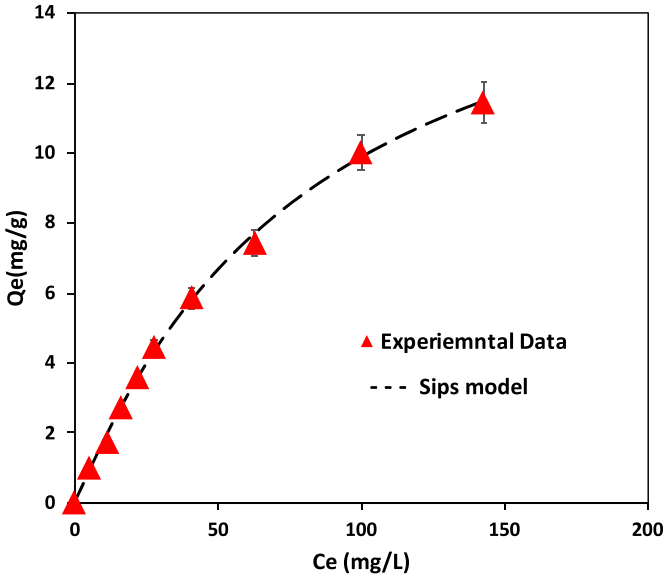

Fig. 6. Adsorption isotherm of chromium (VI) onto adsorbent of silicon dioxide. Adsorbent dose: 0.10 g; shaking rate: 200 rpm; and temperature: 298 K. (For interpretation of the references to colour in this figure legend, the reader is referred to the Web version of this article.)

indicating high level of agreement between the experimental data and the Sips model. Also, the obtained maximum uptake (Q_m) was around 15 mg/g, due to presence of active binding sites (PEI-functionalized nanoparticles) embedded in the Diatomite surface. Furthermore, having heterogeneity coefficient values of unity indicates that the isotherms had a Langmuirian trend, i.e., monolayer adsorption.

3.2. Column adsorption

Fig. 7 shows the obtained breakthrough curves (BTCs) for the

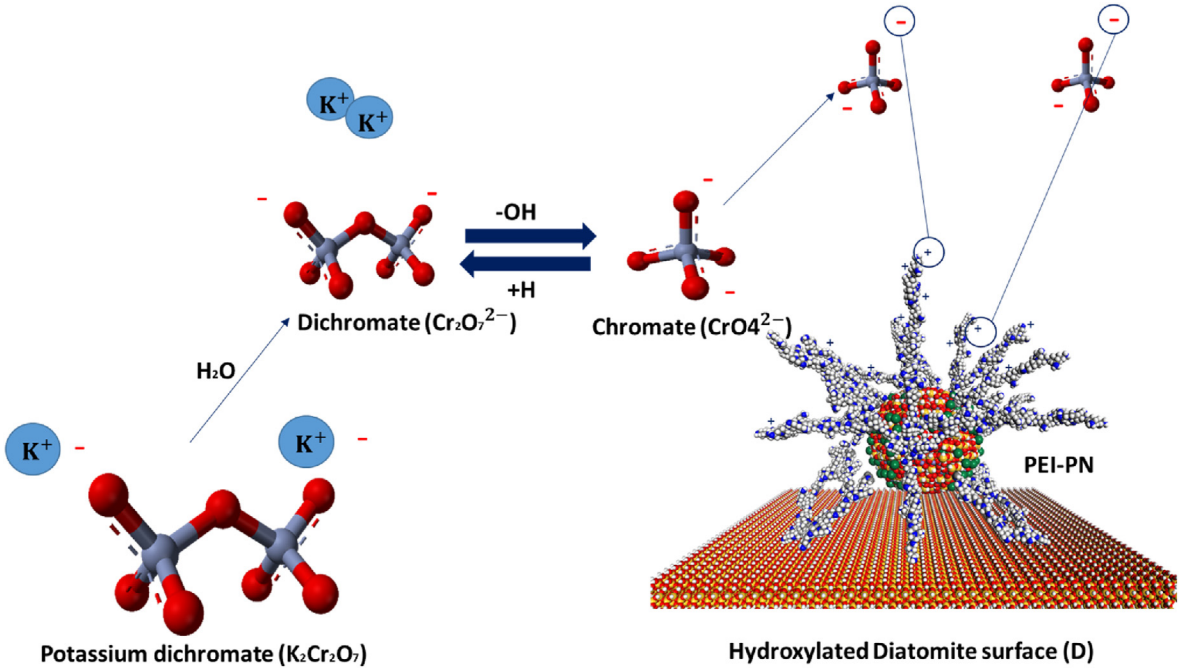

Fig. 5. Pictorial representation of the interaction mechanism of the chromate groups (CrO_4^{2-}) on the functionalized nanoparticles of PEI-PN at pH of 9.

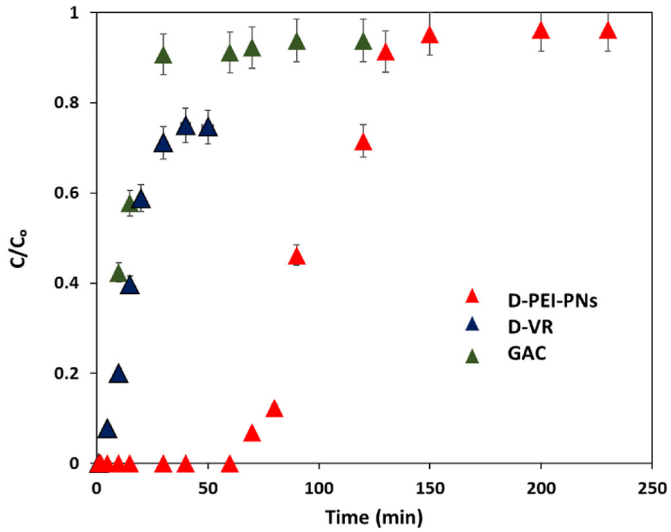

Fig. 7. Experimental BTCs for the adsorption of chromium ion obtained for granulated activated carbon (GAC) in comparison with Diatomite before (D-VR) and after loading the nanoparticles of PEI-PNs (D-PEI-PNs). Experimental operating conditions: Feed concentration = 200 mg/L, flow rate = 1 mL/min, bed height = 7.5 cm, and temperature = 298 K.

Diatomite before (D-VR) and after loading with PEI-PNs (D-PEI-PNs) in comparison with the granulated activated carbon (GAC) at constant operational parameters. As clearly noticed, the best attainment breakthrough time was obtained for D-PEI-PNs with an approximate t_b value of 55 min. While GAC and D-VR had approximate t_b values < 10 min. Accordingly, D-PEI-PNs has the highest uptake and maximum percentage removal of chromium (VI) and hence, it was chosen to study the influence of the other operational parameters (Q, Z and L).

Figs. 8–10a represent the experimental breakthrough curves (BTCs) obtained from the fixed column experiments by varying the influent chromium concentration (C_o), inlet flow rate (Q), and bed-height (L). Figs. 8–10b represent dimensionless analysis (dimensionless time ($\bar{t}$) against normalized concentration ($\bar{C}$)) of the obtained BTC (triangular points) and their fitting with the numerical solution of Equation (10) (dashed lines). Table 4 summarizes the controlled parameters for the obtained BTCs (C_o, Q, and L), the estimated designed parameters (t_b, t_t, *%Removal*, and H_{unb}), and the obtained fitting parameters (Pe_m and Pe_L) from fitting the dimensionless data points with the solution of Equation (9), together with standard error analysis of the fitting in form of χ^2. As listed in Table 4, increasing the chromium flow rate and inlet concertation reduced the values of t_b, t_t, and % removal and their values increased with higher bed-heights. The table also shows the numerical values of the fitting parameters (Pe_m) obtained by fitting the numerical solution of Equation (9) with the experimental BTC, along with the values of Pe_L. As shown in Table 4, the values of Pe_L tend to be close to one in most of the cases, which indicates an equal contribution of convection and axial dispersion rates for chromium adsorption inside the fixed-bed column through changing all the operational parameters (Martin, 1977). These results are not in agreement with our previous study, which showed high values of Peclet number in removing the total organic carbon (TOC) even with using the same sorbent, especially at high flow rates (Hethnawi et al., 2017a). These results prove that different molecules have different diffusion resistance, e.g., transporting big molecules like TOC through the column would provide high diffusional resistance, leading to low molecular diffusion and high value of Pe_L. Dichromate molecules, on the other hand, are smaller and thus, expected to have faster diffusion inside the column, resulting in high contribution of diffusion rate, as the limiting mass transfer phenomenon, and as a result, low values of Pe_L (see Table 5).

3.2.1. *Effect of feed concentration*

As one of the limiting factors and a primary process variable, the effect of chromium (VI) inlet concentration on the breakthrough profiles was analyzed for chromium (VI) concentrations of (100, 150, and 200 mg/L) with constant flow rate (1 mL/min) and bed-height (7.5 cm) (Fig. 8). As expected, by increasing the inlet chromium (VI) concentration, a smaller volume of the effluent can be treated by the *fixed* mass of the adsorbent (Hethnawi et al., 2017a, 2018; Dolatyari et al., 2017). On the other hand, when the inlet concentration of chromium (VI) is low, a late breakthrough time is observed, and a longer time is needed for the sorbent surface to reach saturation. Thus, it can be noticed from Fig. 8 that as the inlet concentration of chromium (VI) increased from 100 to 200 mg/L, a faster breakthrough time and high adsorption uptake are obtained inside the column, due to overcoming the mass transfer resistance, which causes saturation of the limited number of binding sites and resulting in leaving more chromium (VI) molecules un-absorbed in

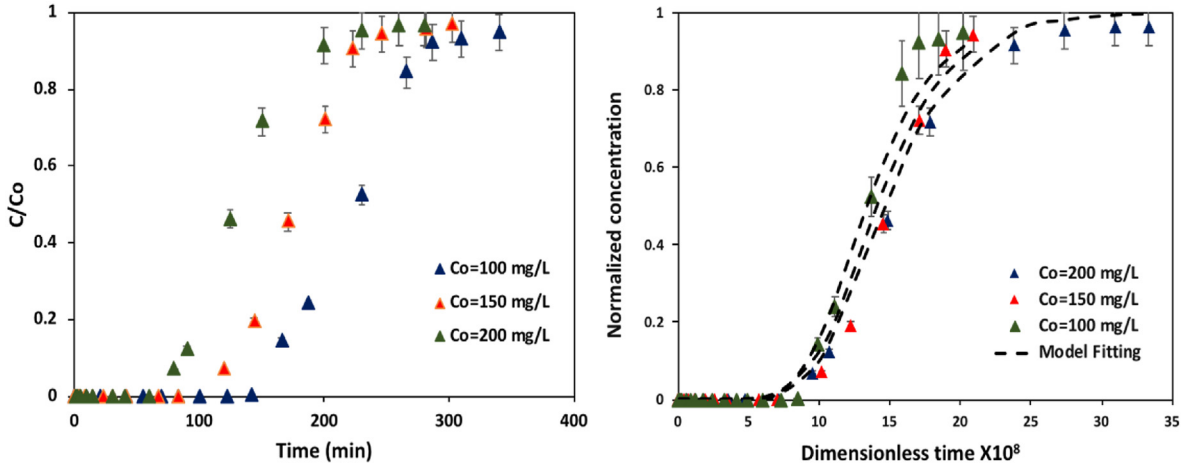

Fig. 8. (a) Experimental BTCs for the adsorption of chromium ion obtained at influent concentrations of 100, 150, and 200 mg/L, and (b) dimensionless analysis of the experimental data (triangular points) together with their fitting with the numerical solution of Equation (10) (dashed lines). Experimental operating conditions: flow rate = 1 mL/min, bed height = 7.5 cm, temperature = 298 K.

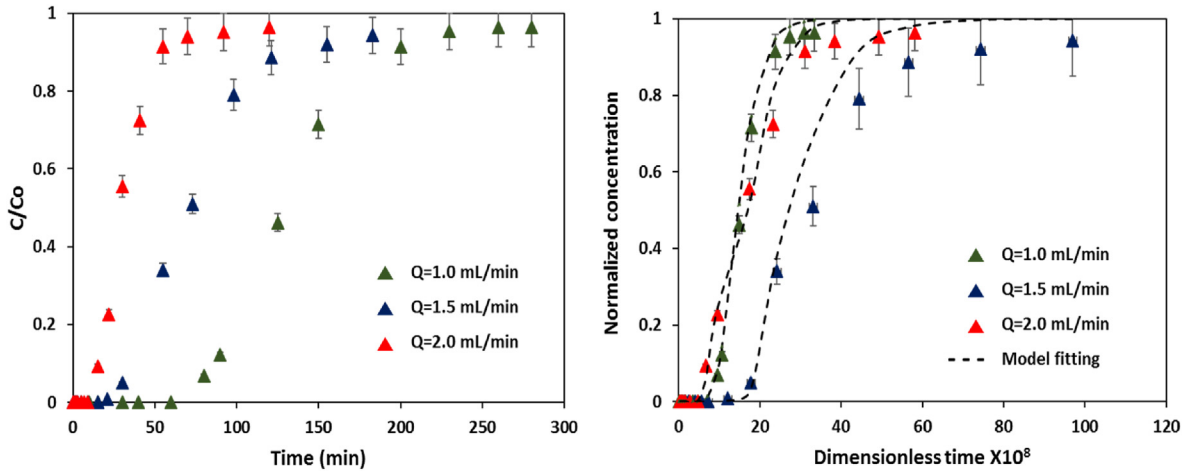

Fig. 9. (a) Experimental BTCs for the adsorption of chromium (VI) ions obtained at inlet flow rates of 1, 1.5, and 2 mL/min, and (b) dimensionless analysis of the experimental data (triangular points) together with their fitting with the numerical solution of Equation (10) (dashed lines). Experimental operating conditions: C_o = 200 mg/L, bed height = 7.5 cm, temperature = 298 K.

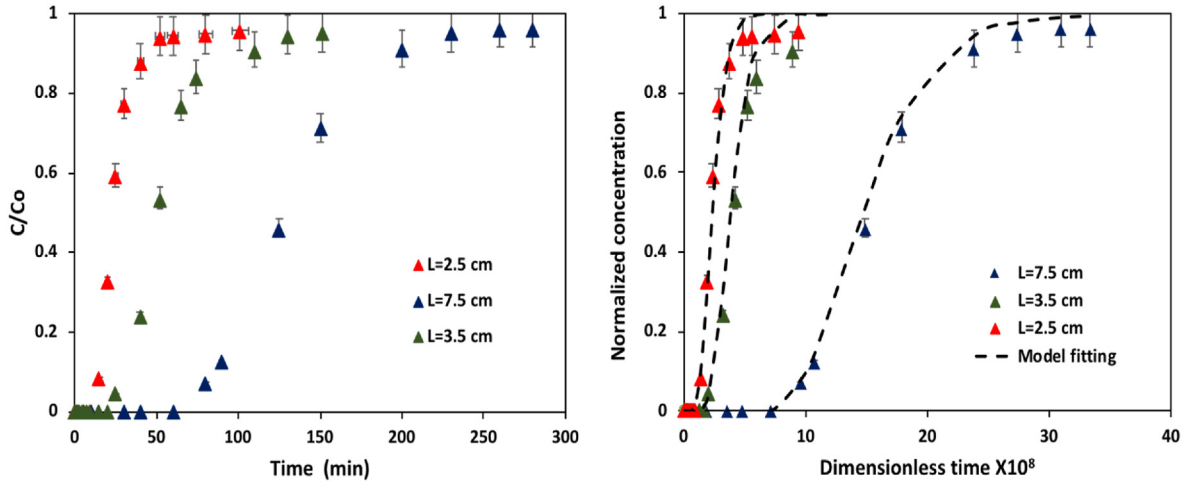

Fig. 10. (a) Experimental BTCs for the adsorption of chromium ion obtained at bed-heights of 2.5, 3.5, and 7.5 cm, and (b) dimensionless analysis of the experimental data (triangular points) together with their fitting with the numerical solution of Equation (10) (dashed lines). Experimental operating conditions: C_o = 200 mg/L, Q = 1 mL/min, temperature = 298 K.

Table 4
Breakthrough curves (BTCs) experimental conditions, designed parameters, fitting parameters with dimensionless convection axial dispersion model together with standard error analysis of the fitting in form of χ^2 for chromium adsorption inside the fixed bed column.

Experimental conditions			Designed parameters				Fitting parameters		Error analysis
Q (ml/min)	C_o (ml/L)	L (cm)	t_b (min)	t_t (min)	%Removal	H_{unb} (cm)	$Pe_m \times 10^{-4}$	Pe_L	$\chi 2$
1.0	100	7.5	270	281.6	82.50	0.43	6.28	5.64	0.03
1.0	150	7.5	210	247.5	80.45	1.59	4.40	3.93	0.11
1.0	200	7.5	180	218.5	78.03	1.85	3.40	2.81	0.02
1.5	200	7.5	130	207.0	62.10	2.28	2.35	2.12	0.01
2.0	200	7.5	50.0	61.75	51.40	4.45	0.92	0.83	0.04
1.0	200	2.5	48.0	54.45	45.50	1.75	4.00	1.19	0.07
1.0	200	3.5	75.0	90.00	50.00	0.88	4.63	1.93	0.05

the solution. Presence of more un-adsorbed chromium (VI) ions provided less residence time and high rate of mass transfer. This consequently led to an increase in the diffusivity and the axial dispersion, which, in term of dimensionless number analysis, led to a decrease in the value Pe_L

3.2.2. Effect of inlet flow rate

Fig. 9 shows the breakthrough data obtained by changing the flow rate from 1 to 2 mL/min at constant bed height (7.5 cm) and chromium inlet concentration (200 mg/L). As seen, increasing the fluid velocity led to reducing the breakthrough time and decreasing removal efficiency of chromium (VI). When chromium (VI) enters

Table 5
Adsorption-desorption parameters for the chromium removal through the three backwash cycles.

Regeneration cycle number	t_b	ER%
1	180	100
2	180	98
3	179	96

the column at high speed, the available binding sites can be occupied at less time, and thus the column get saturated faster and the chromium-adsorbent contact time is reduced (Hethnawi et al., 2017a, 2018; Dolatyari et al., 2017). With less residence time, mass transfer rate increases when the flow rate increases, and the BTC became steeper, i.e., the breakthrough time and adsorbed chromium ions decrease. Inside the column, the residence time of chromium ions was short for attaining the adsorption equilibrium at high flow rate, and as a result, the front of the mass transfer zone reached to the bottom of the column quickly, causing early saturation of the column, and leaving more un-adsorbed chromium ions from the column. This caused significant reduction in the removal efficiency. Thus, with having high flow rate, the residence time for the chromium ions inside the column is reduced. This leads to reduce the rate of diffusion and axial dispersion that subsequently contributed in reduction of Pe_L as shown in Table 4 (Hethnawi et al., 2017a, 2018; Dolatyari et al., 2017).

3.2.3. Effect of bed height

Accumulation of chromium ions is highly dependent on the quantity of the adsorbent inside the column (bed-height). To study the effect of bed height on the BTC, chromium (VI) ion solution with constant influent concentration of 200 mg/L and flow rate of 1 mL/min was passed through the column at different bed heights (Hethnawi et al., 2017a, 2018; Dolatyari et al., 2017). Fig. 10 shows the performance of BTC at column depths of 2.50, 3.50, and 7.50 cm. The results revealed that the dimensionless breakthrough time increased with increasing bed height, due to having higher bed capacity in presence of more sorption sites. As seen, the behavior of the BTC profile at different lengths was similar, which confirms having identical axial dispersion values in the absence of back mixing. Thus, there is no presence of any relevant difference when the general mass balance is applied in a small or in large column under the same operational conditions (Hethnawi et al., 2017a, 2018; Dolatyari et al., 2017). At high bed depth, more amounts of sorbent and binding site area available, which provide more residence time for the chromium ions to interact with the available PEI-PN. Consequently, the value of axial Pe_L tends to increase linearly with increasing the column depth, such that the effect of axial dispersion is minimal, except when the bed is short for any commercial packed-bed column operating under practical Reynold number (R_e). This justifies the use of a plug-flow assumption in the simulation of short fixed-bed column.

3.3. Desorption and regeneration study

As pH plays role in the adsorption of chromium on D-PEI-PN, the desorption of the spent material is considered an important aspect. As shown in Section 3.2, low adsorption capacity of chromium was obtained at low pH (pH < 6), indicating the possibility to reverse the adsorption process through passing the spent material in regenerating cycles. Fig. 11 represents the adsorptive and desorptive breakthrough curves for the saturated column of D-PEI-PN that were achieved through running three successive backwashing cycles with 0.05 mM of HNO_3 at pH 5. At low pH, the

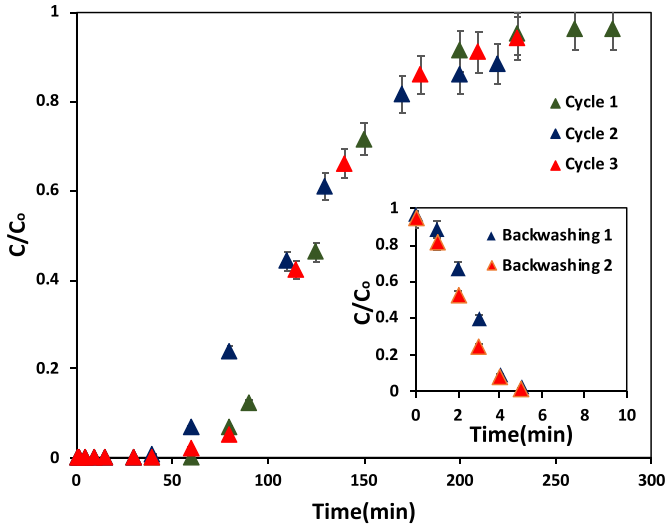

Fig. 11. Reusability of D-PEI-PN for adsorption and desorption of chromium from wastewater during three regenerative cycles. Adsorption: C_o = 200 mg/L, Q = 1 mL/min, and Z = 7.5 cm. Desorption: 0.05 mM of HNO_3 at pH of 5 and Q = 1 mL/min.

chromium ion is desorbed and the PEI-PN tends to be protonated rapidly (<10 min) with an identical breakthrough behavior of D-PEI-PN after every regeneration cycle. These results are also confirmed by Table 3 that shows similar values of tb and ER%. Thus, the adsorption capacity of D-PEI-PN for removal of chromium ions remains unaffected after the regeneration. Also, D-PEI-PN can be considered as a good candidate for continuous removal of chromium ions from wastewater.

3.4. Application to real tannery wastewater

After showing the capabilities of D-PEI-PN in removing chromium (VI) ions from synthetic wastewater sample through batch and continuous fixed-bed column, the performance towards removal of chromium ions from a real sample is verified. From the ICP-OES analysis, the real tannery wastewater sample contains chromium, nickel, and lead as shown in Table 6. The concentration of chromium (VI) reached up to 203 mg/L. The other metals had very low concentrations in the tannery wastewater sample.

FTIR analysis (Fig. 12) was also carried out on the sample to check if there is any organic compounds that might be bonded to the chromium present in the wastewater sample. As shown from the FTIR spectrum, a band is obtained at region 600–700 cm $^{-1}$, which is attributed to presence of C–S linkage. The band obtained between 1020 and 1220 cm^{-1} is assigned to alkyl amine. The obtained bands at regions of 1430-1420, 1510, 1610 cm^{-1} are attributed to stretching vibrations of aromatic C=C, and C=O, respectively (Aging and Munajad, 2018), where the band at range between 2850 and 2950 cm^{-1} is attributed to C–H stretching vibration. Thus, the chromium ion present in the real tannery sample could be bonded to alkyl, alkyl-amine, or phenolic compounds. After characterizing the tannery sample, chromium removal efficiency test was performed continuously inside the fixed-bed column by using diatomite before and after functionalizing it with PEI-PNs. Both tests were performed at inlet flow rate, initial chromium concentration, and bed height of 1 mL/min, 203 mg/L, and 7.5 cm, respectively.

Fig. 13 shows the BTCs for both tests and the obtained designed parameters of t_b and t_t for chromium (VI) are listed in Table 7. As seen, the values of t_b and t_t are much higher than that obtained for

Table 6
ICP-EOS elemental analysis for chromium (VI), nickel, and lead for the real tannery wastewater.

Chromium (VI)		Nickel		Lead	
Concentration (mg/L)	Concentration RSD	Concentration (μg/L)	Concentration RSD	Concentration (μg/L)	Concentration RSD
203	1.34	11.98	1.05	0.00	N/A

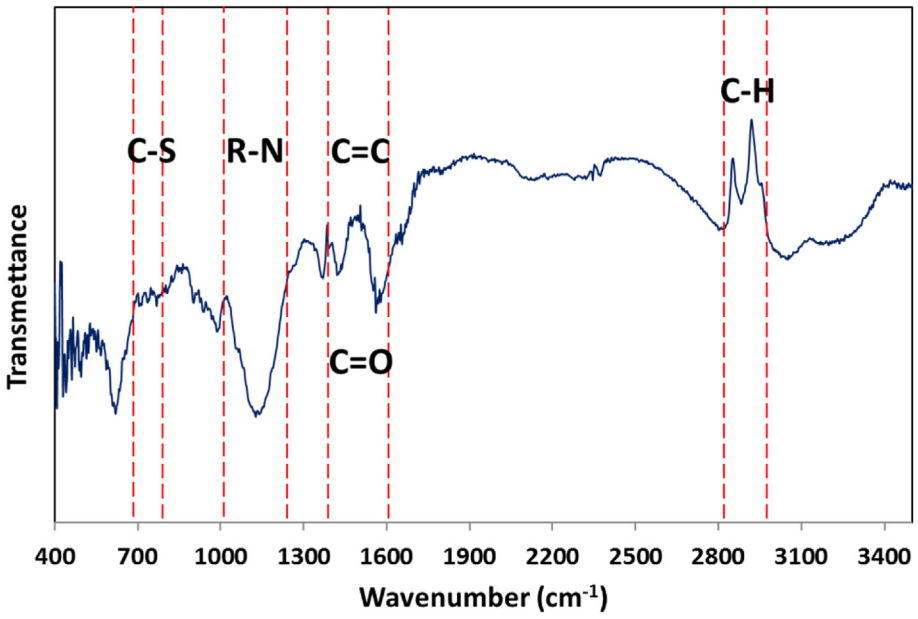

Fig. 12. FTIR spectrum for the dried wastewater sample of tannery at framework region 400-3400 cm^{-1}.

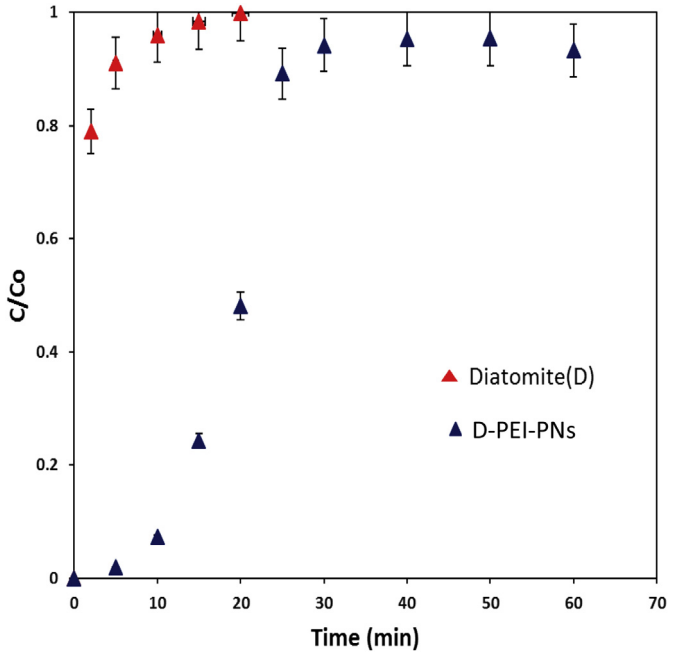

Fig. 13. Experimental BTCs for the adsorption of chromium ion from real tannery wastewater by using the Diatomite and D-PEI-PNs at C_o = 203mg/L, Q = 1 mL/min, bed height = 7.5 cm.

Table 7
Breakthrough curves (BTCs) experimental conditions and designed parameters for chromium (VI) adsorption from the real tannery wastewater inside the fixed bed column.

Adsorbent	Experimental conditions			Designed parameters	
	Q (mL/min)	C_o (mg/L)	L (cm)	t_b (min)	t_t (min)
Diatomite	1.0	203	7.5	2	3.50
D-PEI-PNs	1.0	203	7.5	10	27.5

standalone Diatomite, without nanoparticles.

4. Conclusion

A commercial filter aid material was modified with polyethylenimine-functionalized pyroxene nanoparticles for removing chromium (VI) from synthetic and real tannery wastewater. The adsorption experiments were performed in batch process followed by continuous fixed-bed column experiments. The performance of fixed-bed column adsorption was dependent on flow rate, bed height, and initial chromium (VI) concentration. Higher adsorption efficiency was observed at lower inlet concentration, lower flow rate, and higher adsorbent bed height. The adsorption inside the column was satisfactorily described by a dimensionless form of the convection-axial dispersion kinetic model under different values of operational parameters (i.e., inlet flow rate, initial concentration, and bed-height). Experimental data were fitted to the convection-axial dispersion dimensionless

model, with Peclet number being the fitting parameter. Based on the values of Peclet number, the model predicts the mass transfer rate limiting step (diffusion or convection, under the influence of flow or concentration gradient via advection and axial dispersion phenomena). The obtained Peclet number values tend to be close to one in most of the cases, which indicates an equal contribution of advection and axial dispersion rates for chromium adsorption inside the fixed-bed column through changing all the operational parameters. The model also involves the kinetic parameters obtained from the equilibrium batch adsorption experiment, which was described by the Sips model. At equilibrium, the batch adsorption study showed maximum uptake around 15 mg/g, due to presence of active binding sites (PEI-functionalized nanoparticles) embedded on the Diatomite surface. Furthermore, having heterogeneity coefficient values of unity indicates that the isotherms had a Langmuirian trend, i.e., monolayer adsorption. This study contributes to the evolution of nanoparticle technology in cleaning up industrial effluents. It also sheds some lights on integrating nanoparticles in granular bed-filtration for combining filtration and adsorption processes into one process for cost-effectively cleaning up industrial effluents.

CRediT authorship contribution statement

Afif Hethnawi: Conceptualization, Methodology, Data curation, Writing - original draft. **Wisal Khderat:** Methodology, Visualization, Investigation, Writing - original draft. **Kotaybah Hashlamoun:** Software, Validation. **Amer Kanan:** Supervision. **Nashaat N. Nassar:** Conceptualization, Supervision, Funding acquisition, Project administration, Writing - review & editing.

Acknowledgments

The authors are grateful to the Natural Sciences and Engineering Research Council of Canada (NSERC) (Grant No. RGPIN-2015-05222). A special acknowledgement to Dr. Tobias Fürstenhaupt for access to the Microscopy and Imaging Facility of the Health Science Center at the University of Calgary and Dr. Christopher Debuhr for providing access to the Instrumentation Facility for Analytical Electron Microscopy at the University of Calgary and Dr. Gerardo Vitale for drawing the CPK representation of nanopyroxene and diatomite surface.

References

Aber, S., Mirzajani, V., 2009. Removal of Cr (VI) from polluted solutions by electrocoagulation: modeling of experimental results using artificial neural. Network 171, 484–490. https://doi.org/10.1016/j.jhazmat.2009.06.025.

Agarwal, A., Gupta, P.K., 2015. Adsorption study of Cr (VI) FROM aqueous solution using animal. Bone Charcoal As Low 3, 151–163.

Aging, T., Munajad, A., 2018. Fourier transform infrared (FTIR) spectroscopy analysis of transformer paper in mineral oil-paper composite insulation under accelerated. https://doi.org/10.3390/en11020364.

Aksu, Z., Gönen, F., 2004. Biosorption of phenol by immobilized activated sludge in a continuous packed bed: prediction of breakthrough curves. https://doi.org/10.1016/S0032-9592(03)00132-8, 39-599-613.

Alnajjar, M., Hethnawi, A., Nafie, G., Hassan, A., Vitale, G., Nassar, N.N., 2019. Silica-alumina composite as an effective adsorbent for the removal of metformin from water. J. Environ. Chem. Eng. 7 (3), 102994. https://doi.org/10.1016/j.jece.2019.102994.

Ball, R.D., 2007. Statistical Analysis and Experimental Design. Assoc. Mapp. plants, pp. 133–196.

Benhadji, A., Taleb Ahmed, M., Maachi, R., 2011. Electrocoagulation and effect of cathode materials on the removal of pollutants from tannery wastewater of Rouïba. Desalination 277, 128–134. https://doi.org/10.1016/j.desal.2011.04.014.

Calero, M., 2018. Bioresource Technology Removal of heavy metals from acid mining e ffl uents by hydrolyzed olive cake. Bioresour. Technol. 268, 169–175. https://doi.org/10.1016/j.biortech.2018.07.124.

Call, M.S., Mastral, A.M., Murillo, R., Garc, T., Ayl, E., Navarro, M.V., et al., 2017. Adsorption of phenanthrene on activated carbons: breakthrough curve. modeling 42. https://doi.org/10.1016/j.carbon.2004.04.001, 2009–17.

Chandrasekaran, B., Raghava Rao, J., Sreeram, K.J., Nair, B.U., Ramasami, T., 1999. Chrome tanning: state-of-art on the material composition and characterization. J. Sci. Ind. Res. (India) 58, 1–10.

Cheung, D., 2007. The adverse effects of Le châtelier ' s principle on teacher understanding of chemical. Equilibrium 86. https://doi.org/10.1021/ed086p514.

Coleman, H.W., Steck, W.G., Hurlbut, F.C., 1991. Experimentation and Uncertainty Analysis for Engineers.

Dolatyari, L., Yaftian, M.R., Rostamnia, S., 2017. Fixed-bed column dynamic studies and breakthrough curve analysis of Eu (III) ion adsorption onto chemically modified SBA-15 silica materials. Separ. Sci. Technol. 52, 393–403. https://doi.org/10.1080/01496395.2016.1250781.

Elabbas, S., Ouazzani, N., Mandi, L., Berrekhis, F., Perdicakis, M., Pontvianne, S., et al., 2016. Treatment of highly concentrated tannery wastewater using electrocoagulation: influence of the quality of aluminium used for the electrode. J. Hazard Mater. 319, 69–77. https://doi.org/10.1016/j.jhazmat.2015.12.067.

Fabbricino, M., Naviglio, B., Tortora, G., d'Antonio, L., 2013. An environmental friendly cycle for Cr(III) removal and recovery from tannery wastewater. J. Environ. Manag. 117, 1–6. https://doi.org/10.1016/j.jenvman.2012.12.012.

Foo, K.Y., Hameed, B.H., 2010. Insights into the modeling of adsorption isotherm systems. https://doi.org/10.1016/j.cej.2009.09.013, 156-2-10.

Gheju, M., Balcu, I., Mosoarca, G., 2016. Removal of Cr (VI) from aqueous solutions by adsorption on MnO 2. J. Hazard Mater. 310, 270–277. https://doi.org/10.1016/j.jhazmat.2016.02.042.

Ghorai, S., Pant, K.K., 2005. Equilibrium , kinetics and breakthrough studies for adsorption of fluoride on activated alumina. https://doi.org/10.1016/j.seppur.2004.09.001, 271-265-42.

Hamdaoui, O., Naffrechoux, E., 2007. Modeling of adsorption isotherms of phenol and chlorophenols onto granular activated carbon part II. Models with more than two parameters 147, 401–411. https://doi.org/10.1016/j.jhazmat.2007.01.023.

Han, R., Wang, Y., Zou, W., Wang, Y., Shi, J., 2007. Comparison of linear and nonlinear analysis in estimating the Thomas model parameters for methylene blue adsorption onto natural zeolite in fixed-bed column. J. Hazard Mater. 145, 331–335. https://doi.org/10.1016/j.jhazmat.2006.12.027.

Hethnawi, A., Nassar, N.N., Manasrah, A.D., Vitale, G., 2017. Polyethyleninimine-functionalized pyroxene nanoparticles embedded on Diatomite for adsorptive removal of dye from textile wastewater in a fixed-bed column. Chem. Eng. J. 320, 389–404. https://doi.org/10.1016/j.cej.2017.03.057.

Hethnawi, A., Nassar, N.N., Vitale, G., 2017. Colloids Surf., A 525, 20–30. https://doi.org/10.1016/j.colsurfa.2017.04.067.

Hethnawi, A., Manasrah, A.D., Vitale, G., Nassar, N.N., 2018. Fixed-bed column studies of total organic carbon removal from industrial wastewater by use of diatomite decorated with polyethylenimine-functionalized pyroxene nanoparticles. J. Colloid Interface Sci. 513, 28–42. https://doi.org/10.1016/j.jcis.2017.10.078.

Hmoudah, M., Nassar, N.N., Vitale, G., El-Qanni, A., 2016. Effect of nanosized and surface-structural-modified nano-pyroxene on adsorption of violanthrone-79. RSC Adv. 6, 64482–64493. https://doi.org/10.1039/c6ra05838h.

Hossein, M., Sahlabadi, F., Eslami, H., Taghi, M., 2019. Groundwater for Sustainable Development Removal of Cr (VI) oxoanion from contaminated water using granular jujube stems as a porous adsorbent. Groundw Sustain Dev 8, 319–323. https://doi.org/10.1016/j.gsd.2018.12.001.

Huang, S., Chen, D., 2009. Rapid removal of heavy metal cations and anions from aqueous solutions by an amino-functionalized magnetic. nano-adsorbent 163, 174–179. https://doi.org/10.1016/j.jhazmat.2008.06.075.

Li, Y., Cui, W., Liu, L., Zong, R., Yao, W., Liang, Y., 2016. Applied Catalysis B: environmental Removal of Cr (VI) by 3D TiO 2 -graphene hydrogel via adsorption enriched with photocatalytic reduction. Appl. Catal. B Environ. 199, 412–423. https://doi.org/10.1016/j.apcatb.2016.06.053.

Lofrano, G., Meriç, S., Zengin, G.E., Orhon, D., 2013. Chemical and biological treatment technologies for leather tannery chemicals and wastewaters: a review. Sci. Total Environ. 461–462, 265–281. https://doi.org/10.1016/j.scitotenv.2013.05.004.

Malkoc, E., Nuhoglu, Y., 2006. Cr (VI) adsorption by waste acorn of Quercus ithaburensis in fixed beds. Prediction of breakthrough curves 119, 61–68. https://doi.org/10.1016/j.cej.2006.01.019.

Martin, H., 1977. PECLET NUMBER HEAT AND MASS TRANSFER IN PACKED BEDS.

Menderes, O., 2002. Fundamental Aspects of the Chrome Tanning Reaction.

Mohan, D., Pittman, C.U., 2006. Activated carbons and low cost adsorbents for remediation of tri- and hexavalent chromium from water. J. Hazard Mater. 137, 762–811. https://doi.org/10.1016/j.jhazmat.2006.06.060.

Natale, F Di, Erto, A., Lancia, A., Musmarra, D., 2015. Equilibrium and dynamic study on hexavalent chromium adsorption onto activated carbon. J. Hazard Mater. 281, 47–55. https://doi.org/10.1016/j.jhazmat.2014.07.072.

Nath, K., Saini, S., Sharma, Y.K., 2005. Chromium in tannery industry effluent and its effect on plant metabolism and growth. J. Environ. Biol. 26, 197–204.

Qu, X., Alvarez, P.J.J., Li, Q., 2013. Applications of nanotechnology in water and wastewater treatment. Water Res. 47, 3931–3946. https://doi.org/10.1016/j.watres.2012.09.058.

Saxena, G., Chandra, R., Bharagava, R.N., 2016. Environmental pollution, toxicity profile and treatment approaches for tannery wastewater and its chemical pollutants. In: Reviews of Environmental Contamination and Toxicology. Springer, Cham.

Shahrak, M.N., Ghahramaninezhad, M., Eydifarash, M., 2017. Zeolitic imidazolate framework-8 for efficient adsorption and removal of Cr (VI) ions from aqueous

solution, 9624–34. https://doi.org/10.1007/s11356-017-8577-5.
Stoquart, C., Servais, P., Bérubé, P.R., Barbeau, B., 2012. Hybrid Membrane Processes using activated carbon treatment for drinking water: a review. J. Membr. Sci. 411–412, 1–12. https://doi.org/10.1016/j.memsci.2012.04.012.
Wang, D., He, S., Shan, C., Ye, Y., Ma, H., Zhang, X., et al., 2016. Chromium speciation in tannery effluent after alkaline precipitation: isolation and characterization. J. Hazard Mater. 316, 169–177. https://doi.org/10.1016/j.jhazmat.2016.05.021.
Xin, X., Wei, Q., Yang, J., Yan, L., Feng, R., Chen, G., et al., 2012. Highly efficient removal of heavy metal ions by amine-functionalized mesoporous Fe 3 O 4 nanoparticles. https://doi.org/10.1016/j.cej.2012.01.016, 132-184-140.
Xu, P., Ming, G., Lian, D., Ling, C., Hu, S., Hua, M., 2012. Use of iron oxide nanomaterials in wastewater treatment: a review. Sci. Total Environ. 424, 1–10. https://doi.org/10.1016/j.scitotenv.2012.02.023.
Yunden, G., Kano, N., Kim, H., 2019. The removal of Cr(III) from aqueous solution using modified. Wool 13, 55–61. https://doi.org/10.17265/1934-7375/2019.02.001.